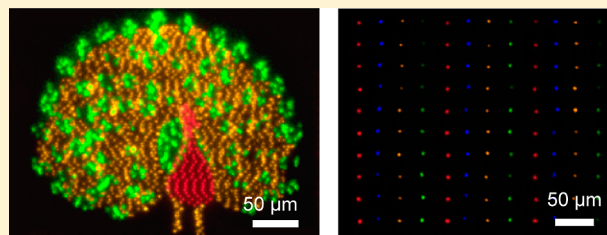


Functional Protein Microarrays by Electrohydrodynamic Jet Printing

Kazuyo Shigeta,^{†,||} Ying He,^{†,||} Erick Sutanto,[‡] Somi Kang,[†] An-Phong Le,[§] Ralph G. Nuzzo,^{†,§} Andrew G. Alleyne,[‡] Placid M. Ferreira,[‡] Yi Lu,^{*,†,§} and John A. Rogers^{*,†,‡,§}[†]Department of Materials Science and Engineering, [‡]Department of Mechanical Science and Engineering, and [§]Department of Chemistry, University of Illinois at Urbana–Champaign, Urbana, Illinois 61801, United States

ABSTRACT: This paper reports the use of advanced forms of electrohydrodynamic jet (e-jet) printing for creating micro- and nanoscale patterns of proteins on various surfaces ranging from flat silica substrates to structured plasmonic crystals, suitable for micro/nanoarray analysis and other applications in both fluorescent and plasmonic detection modes. The approaches function well with diverse classes of proteins, including streptavidin, IgG, fibrinogen, and γ -globulin. Detailed study reveals that the printing process does not adversely alter the protein structure or function, as demonstrated in the specific case of streptavidin through measurements of its binding specificity to biotin-modified DNA. Multinozzle printing systems enable several types of proteins (up to four currently) to be patterned on a single substrate, in rapid fashion and with excellent control over spatial dimensions and registration. High-speed, pulsed operational modes allow large-area printing, with narrow statistical distributions of drop size and spacing in patterns that include millions of droplets. The process is also compatible with the structured surfaces of plasmonic crystal substrates to enable detection without fluorescence. These collective characteristics suggest potential utility of e-jet techniques in wide-ranging areas of biotechnology, where its compatibility with various biomaterials and substrates with different topographies and surface chemistries, and ability to form deposits that range from thick films to submonolayer coatings, derive from the remote, noncontacting physical material transfer mode of operation.



Microarrays are powerful and indispensable tools for modern research in biology and medicine, principally for multiplexed, parallel discovery and assay. Although microarrays consisting of nucleic acids are well-developed and in widespread commercial use, protein microarrays lag far behind in technical maturity and applications, in spite of their significant potential for discovery and understanding of coupling interactions between antibody–antigen, enzyme–substrate, receptor–ligand, aptamer–protein, and protein–protein^{1,2} and for use in biomarker screening.³ These difficulties in realizing the required microarray platforms, in high-resolution configurations formed at high speeds, arise mainly from the intrinsic properties of proteins: they are far less stable than nucleic acids. Currently, protein microarrays are typically formed by in situ protein expression⁴ or by direct spatial patterning, sometimes referred to as spotting,^{5–7} which can be accomplished using techniques such as photolithography,^{8–12} e-beam lithography,¹³ microcontact printing,^{14–27} dip-pen nanolithography^{28–33} and polymer pen lithography,³⁴ inkjet printing,^{35–38} and others that use tools such as the contact printing arrayer.³⁹ Although these methods offer many important capabilities, each has some subset of disadvantages in speed, resolution, area coverage, substrate compatibility, convenience in use, cost of operation, and versatility. As a result, there is room for additional work on strategies for fine patterning of proteins and related biomaterials. Here, we explore advanced, nanoscale implementations of electrohydrodynamic jet (e-jet or EHD jet^{40–43}) printing techniques

for this class of application. The e-jet printing method is similar in an operational sense to conventional inkjet printing, in that both rely on droplets ejected from a nozzle toolbit that scans over a substrate of interest. Instead of thermal or acoustic energy as the mechanism for generating these droplets, e-jet exploits electrohydrodynamically induced flows that result from application of an electrical field between the nozzle and substrate. The result is an ability to achieve levels of resolution (i.e., droplet sizes) in e-jet that are 2 orders of magnitude, or more, better than those that are achievable by thermal or piezoelectric inkjet. In fact, previous work demonstrates the ability to print drops with diameters down to ~ 100 nm.⁴⁴ Such capabilities in e-jet printing have been demonstrated with a wide variety of inorganic and polymeric ink materials,⁴⁵ as well as DNA and DNA aptamers.^{44,46}

Although e-jet printing can produce DNA microarrays^{44,46} and protein patterns onto hydrogel substrate for cell culture application,⁴⁷ it has not been explored for more general and more challenging cases in biomaterials, such as proteins, whose structural stability is much worse than DNA, for example, under various conditions of temperatures and pH. In particular, the high voltages (i.e., hundreds of volts) needed for e-jet could, potentially, denature most proteins and thereby diminish their biological functions (i.e., biorecognition) and degrade the

Received: August 26, 2012

Accepted: October 17, 2012

Published: October 17, 2012

printing resolution and fidelity as well. Herein we report e-jet printing of several different proteins onto various solid substrate surfaces, over large areas and at high speeds (1 in. by 1 in. area, with millions of droplets in ~ 15 min) by employing a high-speed pulsed printing technique.⁴⁸ Wide ranging patterns, including those that embed multiple classes of protein in a single printing sequence, can be achieved, with excellent control over the large area spatial uniformity, as well as the statistical distributions in drop size and spacing, with dimensions in the submicrometer regime. The mode of physical mass transfer also allows use of substrates with substantial surface roughness and texture, thereby creating the potential for plasmonic and nonfluorescent modes of detection, as illustrated for specific cases reported here. Binding assays exploiting these capabilities demonstrate that one of the key biological functions, i.e., biorecognition, in the printed proteins is retained.

EXPERIMENTAL SECTION

Materials. Alexa 546 and biotin-labeled DNA with HPLC purity were obtained from Integrated DNA Technologies, Inc. (Coralville, IA, USA). The sequence is 5' biotin-ACT CAT CTG TGA AGA GAA CCT GGG GGA GTA TTG CGG AGG AAG GT-Alexa546 3'. Streptavidin (66 kDa), purified mouse IgG, rabbit IgG (~ 150 kDa), secondary antibody donkey antimouse IgG-Alexa 350, and goat antirabbit IgG-Alexa 546 (~ 150 kDa, 5–6 fluorophore per protein) were purchased from Invitrogen (Carlsbad, CA, U.S.A.). Streptavidin-fluorescein and streptavidin-Cy5 were ordered from GE Healthcare (Piscataway, NJ, U.S.A.). All the antibodies used here are polyclonal. The mCherry fluorescent protein was expressed and purified in the lab. Silicon wafers were purchased from WRS Materials (Spring City, PA, U.S.A.). The e-jet nozzles were obtained from World Precision Instruments (Sarasota, FL, U.S.A.) and then coated with Ti/Au. As a reagent to fluorinate the nozzles, 1H,1H,2H,2H-perfluorodecane-1-thiol, was purchased from Fluorous Technologies Inc. (Pittsburgh, PA, U.S.A.). Glass microscope slides were ordered from Fisher Scientific (Pittsburgh, PA, U.S.A.). Poly(dimethylsiloxane) (PDMS, Sylgard 184) was obtained from Ellsworth Adhesives (Germantown, WI, U.S.A.). Norland optical adhesive 73 (NOA 73) was purchased from Norland Products (Cranbury, NJ, U.S.A.). Fibrinogen, γ -globulin from bovine blood, 4,4'-dithiodibutyric acid, *N*-(3-dimethylamino-propyl)-*N*'-ethylcarbodiimide hydrochloride (EDC), *N*-hydroxysuccinimide (NHS), 2-(*N*-morpholino)ethanesulfonic acid (MES), and 3-glycidoxypropyltrimethoxysilane (epoxy silane) were purchased from Sigma-Aldrich (St. Louis, MO, U.S.A.). All other chemicals were purchased from Sigma-Aldrich (St. Louis, MO, U.S.A.) without further purification.

Nozzle Preparation. Nozzles made of borosilicate glass with inner diameters at the tips of 500 nm, 1, 2, or 5 μ m (TIP05TW1F-L, TIP1TW1-L, TIP2TW1-L, or TIP5TW1-L) were sputter-coated with gold/palladium to a thickness of ~ 14 nm (Desk II TSC, Denton Vacuum, Moorestown, NJ, U.S.A.), immersed into an *N,N*-dimethylformamide (DMF) solution of 0.1 wt % 1H,1H,2H,2H-perfluorodecane-1-thiol for 10 min, dipped in DMF for 10 s, and then dried in air.

E-jet Printing for Single-Protein Microarrays. Voltage was applied between a metal-coated nozzle and a grounded substrate with an amplifier (Agilent Technologies, Santa Clara, CA, U.S.A.) at a standoff height of about 30 μ m. The position of the substrate relative to the nozzle was controlled by a five-

axis stage, i.e., *x*, *y*, and *z* axes, and the two tilting axes (Aerotech, Pittsburgh, PA, U.S.A.). Coordinated control of the entire system was achieved using LabVIEW programs. Proteins with fluorophores (streptavidin-fluorescein and streptavidin-Cy5) were directly printed onto a SiO₂-deposited silicon wafer if no further incubations were needed since they could be directly imaged by fluorescence microscopy. For protein functional arrays (streptavidin/biotin DNA recognition and antibody array applications), since incubation and washing steps are necessary, proteins were printed onto an epoxy-silane-treated surface to facilitate strong binding. For epoxy surface modification, an epoxy silane coupling agent was dissolved in an ethanol solution containing 5% water (v/v, pH 5) with stirring to a final concentration of 2% (v/v). Reactive silanols were formed after 5 min of hydrolysis at room temperature. The substrate was exposed to the silane solution at 35 °C for 14 h, then washed twice with ethanol and once with water to remove excess silane. Finally, the organosilane-modified substrate was cured by incubation at 110 °C for 10 min.

E-jet Printing for Multiple Protein Microarrays. The tool in this case exploited a multinozzle printhead, with four separate ink chambers and nozzles in a rotary arrangement. The first, second, third, and fourth inks were printed individually by rotating the head. The substrate was mounted onto a LabVIEW-controlled two-axis (*x* and *y* axes) stage and a set of three, manually controlled axes (*z* and the two tilting axes in the *x* or *y* axes). For three-component fluorescent protein array printing, 5 μ M streptavidin-Cy5, 10 μ M streptavidin-fluorescein, and 4 μ M goat antirabbit IgG-Alexa 546 in buffer containing 25 mM potassium phosphate (pH 6.9) and 50 mM NaCl with 40% (v/v) glycerol and 0.05% (v/v) Tween 20 were used. For four-component fluorescent protein array printing, 5 μ M each of mCherry, streptavidin-fluorescein, and streptavidin-Cy5 and 4 μ M donkey antimouse IgG-Alexa 350 in buffer containing 25 mM potassium phosphate (pH 6.9) and 50 mM NaCl with 40% (v/v) glycerol and 0.05% (v/v) Tween 20 were used.

Biotin-DNA Incubation for Streptavidin Arrays. For studies of streptavidin-biotin recognition in printed arrays, 5 μ M streptavidin-fluorescein in buffer containing 25 mM potassium phosphate (pH 6.9) and 50 mM NaCl with 40% (v/v) glycerol and 0.05% Tween 20 (v/v) was printed on an epoxy-silane-modified SiO₂/Si surface. A target DNA solution labeled with both Alexa 546 and biotin was then applied to the streptavidin microarray. For the incubation step, 20 μ L of 5 μ M fluorophore and biotin-labeled DNA in 1 \times phosphate-buffered saline (PBS) buffer and 500 mM NaCl were cast onto the printed area and incubated for 30 min in a humidity chamber to prevent the drying during incubation. Next, the substrate was washed with 3–4 mL of deionized (Millipore) water to remove the unbound DNA and extra salt solution and then dried with air.

Secondary Antibody (Anti-IgG) Incubation for Primary Antibody (IgG) Arrays. For antibody array printing, 2 μ M of each primary antibody in buffer containing 25 mM potassium phosphate (pH 6.9) and 50 mM NaCl with 40% (v/v) glycerol and 0.05% (v/v) Tween 20 was printed on an epoxy-silane-modified SiO₂ surface. Then, the IgG pattern was passivated with 5 mg/mL bovine serum albumin (BSA) solution in 1 \times PBS for 20 min, washed with deionized water (Millipore), and dried by air. Finally, the treated pattern was incubated with a mixture of secondary antibody for 40 min, washed with deionized water, and dried by air.

Fluorescence Microscope Imaging. A Zeiss Axiovert 200 M microscope was used for all imaging. DAPI, FITC, rhodamine, and Cy5 filter channels were used for fluorophores Alexa 350, fluorescein, Alexa 546, and Cy5, respectively.

Analysis of Droplet Sizes and Spacings in Patterns E-jet Printed with a 2 μm Nozzle. Fluorescence microscope images of printed and incubated droplets were analyzed with the software package NI Vision Assistant. To distinguish all of the printed droplets from the background, the minimum and maximum values in a histogram were adjusted to select pixels having distinct regions based on a grayscale threshold value. This process converted the original image into a binary image comprising pixels with a common color, corresponding to the selected droplets; other pixels correspond to the background. The number of pixels and position of each droplet from selected regions of the image were analyzed with the software. The spacing between adjacent droplets was calculated from the two distances (x and y axis direction). The calculated spacing and area were analyzed with LabVIEW to generate histograms.

Analysis of Droplets E-jet Printed with a 500 nm Nozzle. An atomic force microscope (AFM, MFP-3D Stand Alone AFM, Asylum Research, Santa Barbara, CA, U.S.A.) was used to analyze droplets printed with 500 nm nozzles. The first step involved flattening the entire image to first order, to subtract effects of substrate tilt. Next, three-dimensional and cross-sectional images were created. The measured height profiles were fit to Gaussian forms in LabVIEW, as a way to extract quantitative information on shapes and sizes.

Fabrication of Plasmonic Crystal Substrates. Plasmonic crystals were fabricated with the techniques of soft nanoimprint lithography, using methods described in detail elsewhere.⁴⁹ A PDMS stamp for this purpose was placed against a layer of urethane prepolymer (NOA 73) cast on a glass slide. The prepolymer was cured by passing ultraviolet light through the stamp while in contact. Peeling the stamp away left an embossed pattern of relief on the polymer, in a geometry matching that of the stamp whose nanowell diameter and center-to-center spacing were 420 and 740 nm, respectively. Next, gold (32 nm in thickness) was deposited onto the polyurethane surface by sputtering (AJA International) at 5 mTorr in argon. The resulting substrate was immersed in an ethanolic solution of 33 mM 4,4'-dithiodibutyric acid for 14 h to obtain a carboxyl-terminated self-assembled monolayer (SAM) on the surface. Then, the substrate was rinsed with ethanol and dried by air. After the carboxyl-terminated SAM was activated by EDC (200 mM)/NHS (50 mM) in 50 mM MES buffer solution (pH = 5.5) for 15 min, the surface was rinsed with water and dried by air.

Optical Microscope Observation of Antibodies E-jet Printed onto Plasmonic Crystal Surfaces. A Zeiss Axiovert 200 M microscope with a band-pass filter at 610–700 nm was used for imaging. Fibrinogen and γ -globulin solutions were printed on plasmonic crystals and washed with PBS buffer to obtain monolayer of the printed antibodies. For normalization, the optical micrographs of the printed and washed surfaces were divided by images of a bare glass substrate collected with the same band-pass filters using the software package ImageJ. Images processed in this way were analyzed by histogram expansion with Matlab to illustrate relative heights of the images, i.e., the minimum and maximum values in a histogram in which the intensities were binned into two values.

RESULTS AND DISCUSSION

Figure 1a presents a schematic diagram of a single-nozzle e-jet printer. The printing of proteins is accomplished by applying a

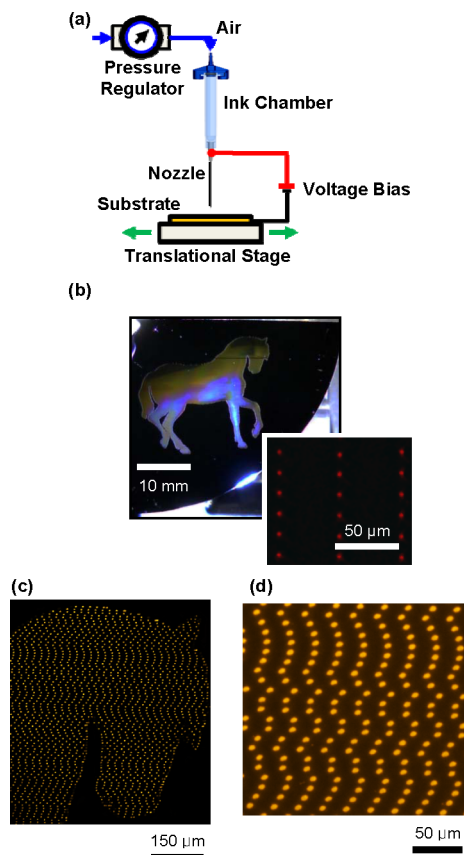


Figure 1. (a) Schematic diagram of an e-jet printer. Voltage applied between a conductive nozzle, with inner diameter between 100 nm and 30 μm , and a substrate on a translational stage affects the printing. (b) Picture of a large-area protein microarray formed by e-jet printing, consisting of nearly 0.5×10^6 dots of streptavidin–Cy5 [5 μM in buffer including 40 vol % glycerol, 0.05 vol % Tween 20, 50 mM sodium chloride, and 25 mM potassium phosphate (pH = 6.9)] patterned across a 1 in. square area of a fluorinated SiO_2 surface. The printing time was 15 min. The inset shows a magnified fluorescence microscope image of printed droplets (size = $\sim 2.6 \mu\text{m}$). (c) Fluorescence microscope image of a pattern of streptavidin–fluorescein [5 μM in buffer including 40 vol % glycerol, 0.05 vol % Tween 20, 50 mM sodium chloride, and 25 mM potassium phosphate (pH = 6.9)] printed with a 2 μm nozzle on a SiO_2/Si surface modified with an epoxy-terminated silane during continuous, programmed motion of the stage (0.5 mm/s at 20 Hz of pulse width modulation). The results correspond to subsequent incubation with 5 μM biotin labeled with Alexa 546 DNA and collected at the rhodamine channel. (d) Magnified image of panel c. The diameter of the droplets is $\sim 4.5 \mu\text{m}$.

voltage bias between a metal-coated glass capillary nozzle connected to an ink chamber and a grounded substrate at a distance of $\sim 30 \mu\text{m}$ between the nozzle tip and the substrate surface. After filling the nozzle with ink, a small pressure (between 0 and 1 psi, depending on the nozzle diameter) was applied to the ink chamber with a regulated power supply to prepare the system for electrohydrodynamic printing.

To demonstrate the speed, resolution, and area coverage of e-jet printing with a single type of protein, we used streptavidin

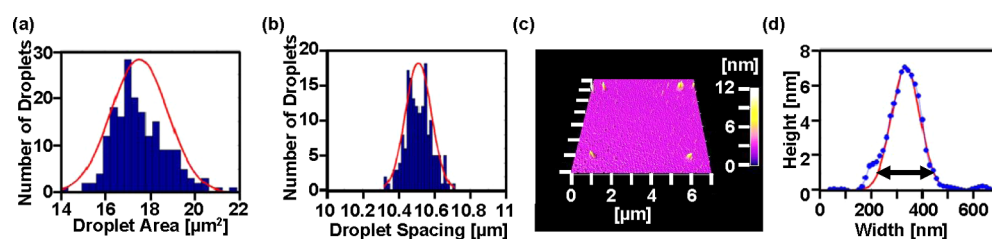


Figure 2. (a) Statistical analysis of the sizes of 189 printed droplets shown in Figure 1d. The red line corresponds to a Gaussian curve whose mean and standard deviation are $17.5 \mu\text{m}^2$ and $1.3 \mu\text{m}^2$ (7.3%), respectively. (b) Statistical analysis of the spacing between adjacent droplets shown in Figure 1d. The red line corresponds to a Gaussian curve whose mean and standard deviation are $10.5 \mu\text{m}$ and 70 nm (0.7%), respectively. (c) AFM image of streptavidin [$2 \mu\text{M}$ in buffer including 40 vol % glycerol, 0.05 vol % Tween 20, 50 mM sodium chloride, and 25 mM potassium phosphate (pH = 6.9)] printed on a bare silicon wafer with a 500 nm nozzle in a drop-on-demand mode (dwelling time of the stage = 0.12 s). (d) Cross-sectional height profile of the bottom-right droplet in panel c. The blue dots correspond to the measured height. The red line corresponds to a Gaussian curve whose mean and standard deviation are 340 nm medium and 50 nm, respectively.

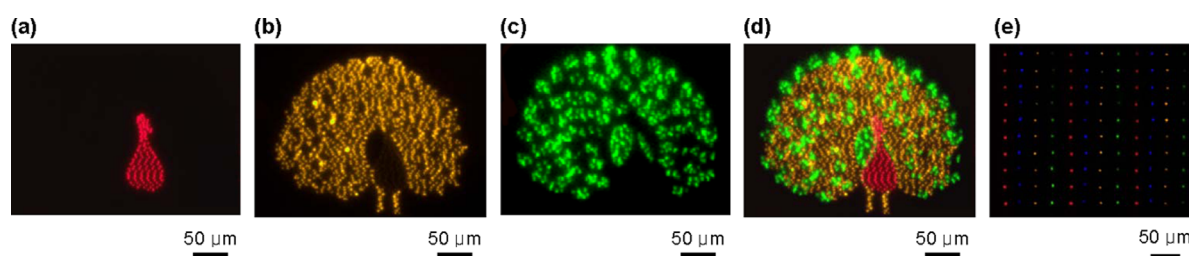


Figure 3. (a–d) Fluorescence microscope images of a peacock pattern formed using three different fluorescently labeled proteins: (a) Streptavidin–Cy5 [$5 \mu\text{M}$ in buffer including 40 vol % glycerol, 0.05 vol % Tween 20, 50 mM sodium chloride, and 25 mM potassium phosphate (pH = 6.9)] printed with a $1 \mu\text{m}$ nozzle on a fluorinated SiO_2 surface and collected using the Cy5 channel of the fluorescence microscope. The diameters of the printed are $\sim 1.1 \mu\text{m}$. (b) Goat anti-rabbit IgG–Alexa 546 ($4 \mu\text{M}$) printed with a $1 \mu\text{m}$ nozzle and collected using the rhodamine channel. The diameters of the droplets are $\sim 1.6 \mu\text{m}$. (c) Streptavidin–fluorescein ($10 \mu\text{M}$) printed with a $1 \mu\text{m}$ nozzle and collected using the FITC channel. The diameters of the droplets are $\sim 1.9 \mu\text{m}$. (d) A composite image generated by overlay of the other frames. (e) Similar overlay of fluorescence microscope images of a four-protein alternating array. Streptavidin–Cy5 ($5 \mu\text{M}$), donkey antimouse IgG–Alexa 350 ($4 \mu\text{M}$), mCherry ($5 \mu\text{M}$), and fluorescein–streptavidin ($5 \mu\text{M}$) in buffer containing 40 vol % glycerol, 0.05 vol % Tween 20, 50 mM sodium chloride, and 25 mM potassium phosphate (pH = 6.9) were printed with $2 \mu\text{m}$ nozzles on a SiO_2 -coated silicon wafer. The images from left to right were collected using the Cy5 (red), DAPI (blue), rhodamine (yellow), and FITC (green) channels, respectively. The average droplet size and standard deviation are 3.4 and $0.6 \mu\text{m}$.

as a prototype with bioconjugation capabilities. To facilitate imaging of the printed patterns, a streptavidin labeled with the fluorophore Cy5, referred to as streptavidin–Cy5 hereafter, was used with a nozzle of $2 \mu\text{m}$ inner diameter. Figure 1b shows a picture of a representative pattern, in the geometry of a horse, formed on a fluorinated SiO_2 surface. A magnified fluorescent microscopic image in Figure 1b, collected using the Cy5 channel of the microscope through a Cy5 filter, indicates average droplet sizes of $\sim 2.6 \mu\text{m}$ and separations of $\sim 17 \mu\text{m}$. The total number of printed droplets in this pattern is nearly 0.5×10^6 (493 000), formed at a frequency of 1000 droplet/s, for a total printing time of $\sim 15 \text{ min}$.

To investigate whether the e-jet printed proteins can retain their function, we examined the properties of patterns of streptavidin–fluorescein formed with a $2 \mu\text{m}$ diameter nozzle on a SiO_2/Si surface modified with epoxy-terminated silane. The printed substrate was incubated with a 44-mer DNA with biotin attached at the 5'-end and Alexa 546 fluorophore at the 3'-end. Fluorescent images of the head and neck parts of the horse (see Figure 1c and its magnified image in Figure 1d), collected using the rhodamine filter channel due to ranges of wavelengths that are similar to those of Alexa 546,⁵⁰ shows that the printed streptavidin can bind biotin that is linked to Alexa 546 through the 44-mer DNA, and thus maintain its biological function. The average droplet diameter is $\sim 4.5 \mu\text{m}$.

To evaluate the printing uniformity quantitatively, statistical analysis was applied to the pattern of 189 droplets shown in

Figure 1d. On the basis of Gaussian fitting (in red) of the droplet areas (Figure 2a), the mean and standard deviation in droplet area are determined to be $17.5 \mu\text{m}^2$ and $\pm 1.3 \mu\text{m}^2$ (or $\pm 7.3\%$), respectively. Similar Gaussian fitting of droplet spacing (Figure 2b) resulted in mean and standard deviation of the droplet spacing as $10.5 \mu\text{m}$ and $\pm 70 \text{ nm}$ (or $\pm 0.7\%$), respectively. These observations demonstrate the high levels of uniformity that can be obtained in e-jet printing of proteins.

The nozzle size, along with certain other parameters associated with printing, determine the droplet size.⁵¹ To further explore the potential in reducing printed droplet size, smaller-sized nozzles, such as $1 \mu\text{m}$ and 500 nm in diameter, were tested. The resulting drop sizes are too small to evaluate using fluorescent techniques. Instead, AFM imaging was used. An AFM image of four streptavidin droplets appears in Figure 2c. The blue dots in Figure 2d correspond to cross-sectional data for the bottom-right droplet in Figure 2c. The measured height of this printed pattern is $\sim 7 \text{ nm}$, which is comparable to the characteristic size of a streptavidin molecule.^{52–54} The Gaussian curve (in red) yields the average and standard deviation of the diameter, i.e., 340 and $\pm 50 \text{ nm}$, respectively. The black arrow indicates the width corresponding to two standard deviations ($\sim 220 \text{ nm}$).

Protein microarrays require many different types of proteins in a single pattern. One option to achieve this objective is to conduct printing in the modes described above multiple times on a single substrate. Preferably, multiple nozzles could be used

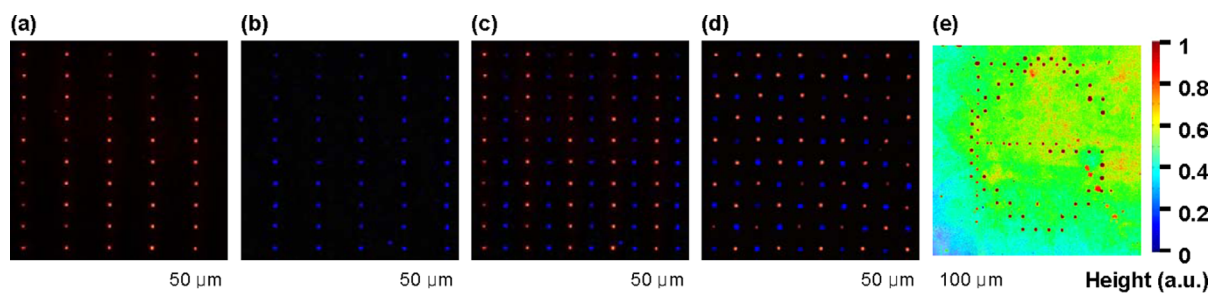


Figure 4. Fluorescence microscope images of two antibody detection microarrays. Mouse IgG and rabbit IgG [each of $2 \mu\text{M}$ in buffer including 40 vol % glycerol, 0.05 vol% Tween 20, 50 mM sodium chloride, and 25 mM potassium phosphate ($\text{pH} = 6.9$)] were printed with $2 \mu\text{m}$ nozzles on a SiO_2 surface modified with epoxy-terminated silane and incubated with a mixture target solution of Alexa 350 donkey antimouse IgG and Alexa 546 goat antirabbit IgG (each of $2 \mu\text{M}$ in $1\times$ PBS buffer, $\text{pH} 7.4$). (a) Alexa 546 signal collected using the rhodamine channel, corresponding to the printed and incubated rabbit IgG. The diameters of the printed and incubated droplets are $\sim 2.5 \mu\text{m}$. (b) Alexa 350 signal collected using the DAPI channel, corresponding to the printed and incubated mouse IgG. The droplet diameters are $\sim 2.2 \mu\text{m}$. (c) Horizontal, alternating pattern consisting of images collected using the rhodamine and DAPI channels (i.e., panels a and b). (d) Diagonal alternating patterns. The ink and incubation conditions here are the same those for panel c. (e) Optical microscope image of a microarray for antibody detection printed on a plasmonic crystal substrate and washed with PBS buffer solution. γ -globulin and fibrinogen [each of $10 \mu\text{M}$ in water including 40 vol % glycerol, 0.025 vol % Tween 20, 50 mM sodium chloride, 25 mM potassium phosphate ($\text{pH} = 6.9$)] printed on a plasmonic surface (whose nanohole period was 740 nm and diameter was 440 nm) on gold/NOA 73/glass and quantitatively analyzed with Matlab program.

to achieve the same outcome, in an automated fashion. Here, we show that multinozzle e-jet print heads can be used for this purpose,⁵⁵ by placing different proteins into different ink chambers and nozzles. After printing one protein in one ink chamber, the multinozzle head rotates to position the next ink chamber above the substrate on which the previous ink was printed. Such a process can be repeated for each ink. Our current system allows printing of up to four different proteins in this manner, although other array geometries can be considered (e.g., linear or matrix arrays of nozzles that can be addressed individually through purely electrical, rather than mechanical, means). As a demonstration of this system, a pattern in the geometry of a peacock was printed with three proteins (streptavidin–Cy5, goat antirabbit IgG–Alexa 546, and streptavidin–fluorescein) using a multinozzle printer. Images collected at the Cy5, rhodamine, and FITC channels of the fluorescence microscope are shown in Figure 3a–c, respectively. Figure 3d corresponds to a composite image that combines the outputs of the three channels. The printed droplet size was ~ 1.1 , 1.6 , and $1.9 \mu\text{m}$ for the streptavidin–Cy5, goat antirabbit IgG–Alexa 546, and streptavidin–fluorescein, respectively. To illustrate registration fidelity, four proteins (streptavidin–Cy5, mCherry, streptavidin–fluorescein, and donkey antimouse IgG–Alexa 350) were printed in a drop-on-demand mode, i.e., in which the exact positions of the printed droplets were controlled by time-gated voltages applied to the nozzle, in a manner coordinated with the stage motion (see Figure 3e for overlay of four fluorescent channels, with micrometer-level registration between the different protein patterns). The dwell time, i.e., time that the voltage was on, for each protein was adjusted to obtain similar sizes in the printed droplets, e.g., the average droplet size and its standard deviation, for each of the four proteins were 3.4 and $0.6 \mu\text{m}$, respectively.

A major application for protein microarrays is in antibody detection. To demonstrate the feasibility of constructing protein chips using the e-jet printer for immunoassays, two nonfluorescent primary antibodies (mouse IgG and rabbit IgG) were printed in the drop-on-demand mode and then incubated with two fluorescently labeled secondary antibodies (donkey antimouse IgG–Alexa 350 and goat antirabbit IgG–Alexa 546).

As shown in Figure 4a, goat antirabbit IgG–Alexa 546 bound to the printed rabbit IgG was detected at the rhodamine channel of the fluorescence microscope, while the bound donkey antimouse IgG–Alexa 350 was detected at DAPI channel, as shown in Figure 4b. Figure 4c is an overlaid image taken at the two channels. As another example, a diagonally ordered array of the antibodies is demonstrated in Figure 4d. These results show that the e-jet printed nonfluorescent primary antibodies can be detected by incubation of the corresponding fluorescently labeled secondary antibodies. In all cases, minimal cross-binding interaction was observed, consistent with the binding specificities between each of the two pairs of primary and secondary antibodies, further demonstrating the retention of protein functionality after printing.

As a final example of versatility of the system, we show that the physical means for mass transfer associated with droplet printing in a technique like e-jet enables patterning on unusual substrates, including those with substantial surface topography. A specific advantage is the capability to print on plasmonically active substrates that can enable optical detection without fluorescent tagging. As a demonstration, we used quasi-3D plasmonic crystals, of the type that are easily fabricated using the techniques of soft nanoimprint lithography, as described in detail elsewhere.⁵⁶ Such plasmonic architectures provide exceptional sensitivity in their optical transmission characteristics to surface-bound species. Here, we e-jet printed monolayers of two proteins (fibrinogen and γ -globulin) onto the plasmonic crystals in geometries of the letters “F” and “G”, respectively, and then washed with a buffer solution. Under an optical microscope, letters “F” and “G” were observed clearly (Figure 4e), consistent with expectation based on the sensitivity of these substrates. On the basis of separate measurements on 3.5 and 2.7 nm thick layers of fibrinogen and γ -globulin, respectively, prepared on a similar plasmonic crystal substrate by a microfluidic device,⁵⁷ we can conclude that the thickness of the e-jet printed droplets observed here are $\sim 3 \text{ nm}$. The height of streptavidin droplets shown in Figure 2c was $\sim 7 \text{ nm}$. As a control, when the same two antibodies were printed onto flat gold/NOA 73/glass substrate, otherwise identical to the plasmonic substrates, no printed dots could be observed. These results confirm the ability for plasmonic crystals to serve as

useful substrates for e-jet printing of protein patterns, due to their nonfluorescent-based imaging modalities.

CONCLUSION

In summary, the results reported here demonstrate that the e-jet printing method can pattern both single types of proteins and multiple proteins over large areas, with high speed and excellent uniformity in droplet size and spacing, with good registration. The printed proteins maintain their biological functions such as ability to bioconjugate to their substrate and to selectively recognize antibodies. The method can be used to print proteins on a variety of solid substrates, ranging from flat silica surfaces to structured plasmonic crystals. With improved engineering implementations having expanded arrays of nozzles and high-speed electronics, the e-jet printing method may have a strong potential for wide application opportunities in printing of advanced protein microarrays for numerous applications in biology and medicine.

AUTHOR INFORMATION

Corresponding Author

*E-mail: yi-lu@illinois.edu (Y.L.); jrogers@illinois.edu (J.A.R.).

Author Contributions

[†]The first two authors contributed equally to this work.

Notes

The authors declare no competing financial interest.

ACKNOWLEDGMENTS

This work was supported by the Center for Nanoscale Chemical Electrical Mechanical Manufacturing Systems at the University of Illinois (funded by the National Science Foundation under Grant CMMI-0749028). We wish to thank Professor Peter Yingxiao Wang for providing mCherry gene and Yang Yu for help in expressing and purifying the mCherry protein. The AFM and fluorescence studies were performed at the facilities in the Frederick Seitz Materials Research Laboratory and Beckman Institute for Advanced Science and Technology at the University of Illinois at Urbana–Champaign.

REFERENCES

- (1) Templin, M. F.; Stoll, D.; Schrenk, M.; Traub, P. C.; Vohringer, C. F.; Joos, T. O. *Trends Biotechnol.* **2002**, *20*, 160–166.
- (2) Zhu, H.; Snyder, M. *Curr. Opin. Chem. Biol.* **2003**, *7*, 55–63.
- (3) Kingsmore, S. F. *Nat. Rev. Drug Discovery* **2006**, *5*, 310–320.
- (4) Chandra, H.; Srivastava, S. *Proteomics* **2010**, *10*, 717–730.
- (5) Ekblad, T.; Liedberg, B. *Curr. Opin. Colloid Interface Sci.* **2010**, *15*, 499–509.
- (6) Wong, L. S.; Khan, F.; Micklefield, J. *Chem. Rev.* **2009**, *109*, 4025–4053.
- (7) Rusmini, F.; Zhong, Z. Y.; Feijen, J. *Biomacromolecules* **2007**, *8*, 1775–1789.
- (8) Liu, Y.; Li, C. M.; Hu, W.; Lu, Z. *Talanta* **2009**, *77*, 1165–1171.
- (9) Waichman, S.; You, C.; Beutel, O.; Bhagawati, M.; Piehler, J. *Anal. Chem.* **2011**, *83*, 501–508.
- (10) Jonkheijm, P.; Weinrich, D.; Koehn, M.; Engelkamp, H.; Christianen, P. C. M.; Kuhlmann, J.; Maan, J. C.; Nuesse, D.; Schroeder, H.; Wacker, R.; Breinbauer, R.; Niemeyer, C. M.; Waldmann, H. *Angew. Chem., Int. Ed.* **2008**, *47*, 4421–4424.
- (11) Huang, Y.-M.; Uppalapati, M.; Hancock, W. O.; Jackson, T. N. *Lab Chip* **2008**, *8*, 1745–1747.
- (12) Alonso, J. M.; Reichel, A.; Piehler, J.; del Campo, A. *Langmuir* **2008**, *24*, 448–457.
- (13) Christman, K. L.; Schopf, E.; Broyer, R. M.; Li, R. C.; Chen, Y.; Maynard, H. D. *J. Am. Chem. Soc.* **2009**, *131*, 521–527.
- (14) Kane, R. S.; Takayama, S.; Ostuni, E.; Ingber, D. E.; Whitesides, G. M. *Biomaterials* **1999**, *20*, 2363–2376.
- (15) Ludden, M. J. W.; Mulder, A.; Schulze, K.; Subramaniam, V.; Tampe, R.; Huskens, J. *Chem.—Eur. J.* **2008**, *14*, 2044–2051.
- (16) Rozkiewicz, D. I.; Kraan, Y.; Werten, M. W. T.; de Wolf, F. A.; Subramaniam, V.; Ravoo, B. J.; Reinhoudt, D. N. *Chem.—Eur. J.* **2006**, *12*, 6290–6297.
- (17) James, C. D.; Davis, R. C.; Kam, L.; Craighead, H. G.; Isaacson, M.; Turner, J. N.; Shain, W. *Langmuir* **1998**, *14*, 741–744.
- (18) LaGraff, J. R.; Chu-LaGraff, Q. *Langmuir* **2006**, *22*, 4685–4693.
- (19) Lahiri, J.; Ostuni, E.; Whitesides, G. M. *Langmuir* **1999**, *15*, 2055–2060.
- (20) Wilhelm, T.; Wittstock, G. *Langmuir* **2002**, *18*, 9485–9493.
- (21) Godula, K.; Rabuka, D.; Nam, K. T.; Bertozzi, C. R. *Angew. Chem., Int. Ed.* **2009**, *48*, 4973–4976.
- (22) Bernard, A.; Delamarche, E.; Schmid, H.; Michel, B.; Bosshard, H. R.; Biebuyck, H. *Langmuir* **1998**, *14*, 2225–2229.
- (23) Coq, N.; van Bommel, T.; Hikmet, R. A.; Stapert, H. R.; Dittmer, W. U. *Langmuir* **2007**, *23*, 5154–5160.
- (24) Howell, S. W.; Inerowicz, H. D.; Regnier, F. E.; Reifenger, R. *Langmuir* **2003**, *19*, 436–439.
- (25) Hyun, J.; Zhu, Y. J.; Liebmann-Vinson, A.; Beebe, T. P.; Chilkoti, A. *Langmuir* **2001**, *17*, 6358–6367.
- (26) Caballero, D.; Samitier, J.; Bausells, J.; Errachid, A. *Small* **2009**, *5*, 1531–1534.
- (27) Inerowicz, H. D.; Howell, S.; Regnier, F. E.; Reifenger, R. *Langmuir* **2002**, *18*, 5263–5268.
- (28) Lee, K. B.; Park, S. J.; Mirkin, C. A.; Smith, J. C.; Mirksich, M. *Science* **2002**, *295*, 1702–1705.
- (29) Lee, K. B.; Kim, E. Y.; Mirkin, C. A.; Wolinsky, S. M. *Nano Lett.* **2004**, *4*, 1869–1872.
- (30) Lee, K. B.; Lim, J. H.; Mirkin, C. A. *J. Am. Chem. Soc.* **2003**, *125*, 5588–5589.
- (31) Lim, J. H.; Ginger, D. S.; Lee, K. B.; Heo, J.; Nam, J. M.; Mirkin, C. A. *Angew. Chem., Int. Ed.* **2003**, *42*, 2309–2312.
- (32) Nam, J. M.; Han, S. W.; Lee, K. B.; Liu, X. G.; Ratner, M. A.; Mirkin, C. A. *Angew. Chem., Int. Ed.* **2004**, *43*, 1246–1249.
- (33) Wilson, D. L.; Martin, R.; Hong, S.; Cronin-Golomb, M.; Mirkin, C. A.; Kaplan, D. L. *Proc. Natl. Acad. Sci. U.S.A.* **2001**, *98*, 13660–13664.
- (34) Zheng, Z. J.; Daniel, W. L.; Giam, L. R.; Huo, F. W.; Senesi, A. J.; Zheng, G. F.; Mirkin, C. A. *Angew. Chem., Int. Ed.* **2009**, *48*, 7626–7629.
- (35) Cook, C. C.; Wang, T. M.; Derby, B. *Chem. Commun.* **2010**, *46*, 5452–5454.
- (36) Pardo, L.; Wilson, W. C.; Boland, T. J. *Langmuir* **2003**, *19*, 1462–1466.
- (37) Arrabito, G.; Musumeci, C.; Aiello, V.; Libertino, S.; Compagnini, G.; Pignataro, B. *Langmuir* **2009**, *25*, 6312–6318.
- (38) Delehanty, J. B.; Ligler, F. S. *Anal. Chem.* **2002**, *74*, 5681–5687.
- (39) MacBeath, G.; Schreiber, S. L. *Science* **2000**, *289*, 1760–1763.
- (40) Galliker, P.; Schneider, J.; Eghlidi, H.; Kress, S.; Sandoghdar, V.; Poulidakos, D. *Nat. Commun.* **2012**, *3*, 890.
- (41) Back, S. Y.; Song, C. H.; Yu, S.; Lee, H. J.; Kim, B. S.; Yang, N. Y.; Jeong, S. H.; Ahn, H. *J. Nanosci. Nanotechnol.* **2012**, *12*, 446–450.
- (42) Duraisamy, N.; Muhammad, N. M.; Ali, A.; Jo, J.; Choi, K.-H. *Mater. Lett.* **2012**, *83*, 80–83.
- (43) Lee, M. W.; Kang, D. K.; Kim, N. Y.; Kim, H. Y.; James, S. C.; Yoon, S. S. *J. Aerosol. Sci.* **2012**, *46*, 1–6.
- (44) Park, J. U.; Lee, J. H.; Paik, U.; Lu, Y.; Rogers, J. A. *Nano Lett.* **2008**, *8*, 4210–4216.
- (45) Park, J. U.; Hardy, M.; Kang, S. J.; Barton, K.; Adair, K.; Mukhopadhyay, D. K.; Lee, C. Y.; Strano, M. S.; Alleyne, A. G.; Georgiadis, J. G.; Ferreira, P. M.; Rogers, J. A. *Nat. Mater.* **2007**, *6*, 782–789.
- (46) Park, J. U.; Lee, S.; Unarunotai, S.; Sun, Y. G.; Dunham, S.; Song, T.; Ferreira, P. M.; Alleyne, A. G.; Paik, U.; Rogers, J. A. *Nano Lett.* **2010**, *10*, 584–591.

- (47) Poellmann, M. J.; Barton, K. L.; Mishra, S.; Wagoner Johnson, A. J. *Macromol. Biosci.* **2011**, *11*, 1164–1168.
- (48) Mishra, S.; Barton, K. L.; Alleyne, A. G.; Ferreira, P. M.; Rogers, J. A. J. *Micromech. Microeng.* **2010**, *20*, 09S026.
- (49) Stewart, M. E.; Mack, N. H.; Malyarchuk, V.; Soares, J. A. N. T.; Lee, T. W.; Gray, S. K.; Nuzzo, R. G.; Rogers, J. A. *Proc. Natl. Acad. Sci. U.S.A.* **2006**, *103*, 17143–17148.
- (50) Panchuk-Voloshina, N.; Haugland, R. P.; Bishop-Stewart, J.; Bhalgat, M. K.; Millard, P. J.; Mao, F.; Leung, W.-Y.; Haugland, R. P. *J. Histochem. Cytochem.* **1999**, *47*, 1179–1188.
- (51) Barton, K.; Mishra, S.; Shorter, K. A.; Alleyne, A.; Ferreira, P.; Rogers, J. *Mechatronics* **2010**, *20*, 611–616.
- (52) Cooper, J. M.; Shen, J.; Young, F. M.; Connolly, P.; Barker, J. R.; Moores, G. J. *Mater. Sci.: Mater. Electron.* **1994**, *5*, 106–110.
- (53) Hendrickson, W. A.; Pahler, A.; Smith, J. L.; Satow, Y.; Merritt, E. A.; Phizackerley, R. P. *Proc. Natl. Acad. Sci. U.S.A.* **1989**, *86*, 2190–2194.
- (54) Weber, P. C.; Ohlendorf, D. H.; Wendoloski, J. J.; Salemme, F. R. *Science* **1989**, *243*, 85–88.
- (55) Sutanto, E.; Shigeta, K.; Kim, Y. K.; Graf, P. G.; Hoelzle, D. J.; Barton, K. L.; Alleyne, A. G.; Ferreira, P. M.; Rogers, J. A. J. *Micromech. Microeng.* **2012**, *22*, 04S008. DOI: 10.1088/0960-1317/22/4/04S008.
- (56) Yao, J. M.; Le, A. P.; Gray, S. K.; Moore, J. S.; Rogers, J. A.; Nuzzo, R. G. *Adv. Mater.* **2010**, *22*, 1102–1110.
- (57) Stewart, M. E.; Yao, J. M.; Maria, J.; Gray, S. K.; Rogers, J. A.; Nuzzo, R. G. *Anal. Chem.* **2009**, *81*, 5980–5989.